creative commons
COMMONS DEED

저작자표시-비영리-변경금지 2.0 대한민국

이용자는 아래의 조건을 따르는 경우에 한하여 자유롭게

- 이 저작물을 복제, 배포, 전송, 전시, 공연 및 방송할 수 있습니다.

다음과 같은 조건을 따라야 합니다:

저작자표시. 귀하는 원저작자를 표시하여야 합니다.

비영리. 귀하는 이 저작물을 영리 목적으로 이용할 수 없습니다.

변경금지. 귀하는 이 저작물을 개작, 변형 또는 가공할 수 없습니다.

- 귀하는, 이 저작물의 재이용이나 배포의 경우, 이 저작물에 적용된 이용허락조건을 명확하게 나타내어야 합니다.
- 저작권자로부터 별도의 허가를 받으면 이러한 조건들은 적용되지 않습니다.

저작권법에 따른 이용자의 권리는 위의 내용에 의하여 영향을 받지 않습니다.

이것은 이용허락규약(Legal Code)을 이해하기 쉽게 요약한 것입니다.

Disclaimer

dCollection

ULSAN NATIONAL INSTITUTE OF
SCIENCE AND TECHNOLOGY

Biocompatible and Flexible Nanogenerators for Wearable and Implantable Mechano-Energy Harvester

Kyeong Nam Kim

Department of Materials Science Engineering

Graduate school of UNIST

2015

ULSAN NATIONAL INSTITUTE OF SCIENCE AND TECHNOLOGY

Biocompatible and Flexible Nanogenerators for Wearable and Implantable Mechano-Energy Harvester

Kyeong Nam Kim

Department of Materials Science Engineering

Graduate school of UNIST

ULSAN NATIONAL INSTITUTE OF
SCIENCE AND TECHNOLOGY

Biocompatible and Flexible Nanogenerators for Wearable and Implantable Mechano-Energy Harvester

A thesis/dissertation
submitted to the Graduate School of UNIST
in partial fulfillment of the
requirements or the degree of
Master of Science

Kyeong Nam Kim

12. 16. 2014
Approved by

_____

Advisor
Jeong Min Baik

ULSAN NATIONAL INSTITUTE OF SCIENCE AND TECHNOLOGY

Biocompatible and Flexible Nanogenerators for Wearable and Implantable Mechano-Energy Harvester

Kyeong Nam Kim

This certifies that the thesis/dissertation of Kyeong Nam Kim is approved.

12. 16. 2014

_____

Advisor: Jeong Min Baik

_____

Soon-Yong Kwon: Thesis Committee Member #1

_____

Ju-Young Kim: Thesis Committee Member #2

ULSAN NATIONAL INSTITUTE OF SCIENCE AND TECHNOLOGY

Abstract

Biodegradable and wearable self-powered devices have represented the emerging technology necessary to new life pattern of human. Silk fibroin-based biodegradable composite-type nanogenerators are demonstrated with controllable lifetime for powering to the implantable devices. The 2D thin film- and 1D wire-type composites consist of the well-dispersed lead-free ferroelectric ($BaTiO_3$, $ZnSnO_3$, $Bi_{0.5}(Na_{0.82}K_{0.18})_{0.5}TiO_3$, and $K_{0.5}Na_{0.5}Nb_{0.995}Mn_{0.005}O_3$) nanoparticles. Ag nanowires are used to enhance the dispersion of the nanoparticles and polyvinylpyrrolidone prevents Ag nanowires from connecting with each other. A maximum output voltages and current densities of 2.2 V and 0.12 $\mu A/cm^2$ in the thin film, and 1.8 V and 0.1 $\mu A/cm^2$ in the wire are obtained under the motion of a foot step for when 30 wt% KNN:Mn nanoparticles are well-dispersed in the solution because of the largest piezoelectric coupling figure of merit. The properties of water-soluble composite films are also controlled with the glycerol up to 48 hrs. And textile structures are desirable for wearable device that are stretchable and flexible. In this article, new textile-structured triboelectric nanogenerators are demonstrated for powering to the wearable devices. The tube structured triboelectric nanogenerator consists of PDMS tube, copper wire in center of device, and aluminum wrapped around the outer surface of tube, which are utilized to generate and harvest triboelectricity. We also fabricate the cable structured triboelectric nanogenerator, which is composed of several tube structured nanogenerator with series connection, resulting in 3 times higher output voltage than that of a tube structured nanogenerator. Additionally, textile- structured triboelectric nanogenerator is fabricated with weaving from numerous tube structured triboelectric nanogenerator with parallel connection to generate high output current. A maximum output voltages and currents of 50 V and 180 μA for the textile-structured nanogenerator are obtained under the vertical stress of pushing tester. Moreover, the relationship between output performance and the amount of deformation at stretchable loading in the stretchable textile structured triboelectric nanogenerator is also investigated. This work should play an important role in new direction to wearable electronics.

ULSAN NATIONAL INSTITUTE OF SCIENCE AND TECHNOLOGY

Contents

ULSAN NATIONAL INSTITUTE OF
SCIENCE AND TECHNOLOGY

ULSAN NATIONAL INSTITUTE OF SCIENCE AND TECHNOLOGY

List of figures

ULSAN NATIONAL INSTITUTE OF SCIENCE AND TECHNOLOGY

Figure 8 (a) The original images indicating the experimental setup for power generation under the foot step in which silk fibroin-based composite-type generator was laid down a woodblock. (b) The output voltage and current density generated from the composite film type nanogenerator with 30 wt% KNN:Mn nanoparticles. (c) The output voltage generated from the devices fabricated using KNN:Mn NPs without and with dispersants in the silk fibroin matrix. The inset indicates the magnified cross-sectional SEM image of the aggregation of the NPs and the well-dispersed NPs. (d) The generated output voltages of the devices fabricated using the different combination of dispersant. The inset shows the current-voltage (I–V) characteristic of only Ag nanowires and Ag nanowires-PVPs composite in the silk matrix films along the vertical direction to identify PVP effect.

Figure 9 The calculated piezopotential difference between of (a) aggregated and (b) well-distributed ferroelectric particles in the silk fibroin matrix.

Figure 10 (a) The output voltages and (b) current densities of the various ferroelectric particles when the concentrations of ferroelectric particles are 30 wt%. The insets illustrate the enlarged graphs of the output signals from the boxed areas

Figure 11 (a) The maintenance time of composite film fabricated with various glycerol concentrations. The left inset shows the photograph of dissolution of the pure silk fibroin film on ITO/PET substrate in distilled water, and the right inset shows the image of insolubility of the film for the compositions of 30wt% glycerol embedded silk fibroin film. The immersion time-dependent change output voltage for (b) the pure silk fibroin-based composite-type film and (c) 30wt% glycerol blend film.

Figure 12 (a) A schematic image and (b) a photograph of silk fibroin-based composite-type wire generator which consists of Al wire, silk fibroin composite layer and aluminum electrode. (c) The output voltage and current density of silk fibroin-based composite-type wire generator.

Figure 13 (a) The fabrication of tube structured triboelectic generator. (b) The SEM image of nanostructured Au coated Al wire and PDMS (c) The output performance of tube structured triboelectric generator with 7 mm diameter of tube. (d) The sealing effect of tube structured triboelectric generator

Figure 14 Mechanism of tube structured triboelectric nanogenerator. (a) Original position of tube strucutured triboelectric nanogenerator. (b) Applied vertical strain results in the contact between PDMS tube and Al wire, generating negative charges on the Al wire and positive charges on the

ULSAN NATIONAL INSTITUTE OF SCIENCE AND TECHNOLOGY

PDMS tube. (c) Separated condition because of withdrawal of the strain. Free electrons flow from back electrode to Al wire. (d) Fully separation of the tube structured triboelectric nanogenerator. (e) Reapplied vertical strain results in the reverse flow of the free electrons.

Figure 15 Cable structured triboelectgric nanogenerator. (a) Photographs of the cable structured triboelectric nanogenerator consisting of 1~3 tube structured triboelectric nanogenerator in parallel connection. (b) output voltage, (c) output current of cable structured triboelectric nanogenerator.

Figure 16 (a) Schematic circuit and (b) image of textile structured triboelectric nanogenerator in parallel connection. (c) Photograph of textile structured triboelectric nanogenerator. (d) Ouput voltage and (e) output current of textile structured triboelectric nanogenerator.

Figure 17 (a) Optical photograph of textile structured triboelectric nanogenerator under the strain 20 % along the both sides direction. (b) Schematic image of diameter change under the stretching. (c) Change of output voltage and output current of textile structured triboelectric nanogenerator.

Figure 18 (a) Output voltage and (b) output current versus the diameter of tube structured triboelectric nanogenerator

ULSAN NATIONAL INSTITUTE OF SCIENCE AND TECHNOLOGY

I. Introduction

Harvesting energy from mechanical energy in our living environment and human body has attracted much attention due to an extended life time, no recharging procedures, and scalability. Since ZnO nanowire arrays have been used to fabricate such piezoelectric nanogenerators [1-6], there have been many attempts to fabricate piezoelectric energy harvesting devices by employing various nanostructured materials such as ZnO [7], $BaTiO_3$ [8], $KNbO_3$ [9], $xKNaNbO_3$-(1-x)$LiNbO_3$ (KNLN) [10], $ZnSnO_3$ [11], and $NaNbO_3$ [12], $0.5Ba(Zr_{0.2}Ti_{0.8})O_3$-$0.5(Ba_{0.7}Ca_{0.3})TiO_3$ (BZT-BCT) [13]. Recently, the polymer-mold-supporting nanogenerators composed of nanowires and nanoparticles have been successfully demonstrated as one of promising platforms for the large-scale and super-flexible nanogenerators. These composite-type nanogenerators are very attractive for large-scale energy harvesting application because of easy fabrication, cost-effectiveness, and mechanical robustness.

Subsequently, various materials and designs of nanogenerators combined triboelectric effect and electrostatic induction have been demonstrated. Triboelectric nanogenerators which are creative developments for harvesting ambient mechanical energy on the basis of the triboelectric effect have shown a significantly high power output to charging lithium ion batteries for portable electronics and wireless sensors. Recently, a various type triboelectric nanogenerators by periodic vertical contact separation, in-plane sliding and rotating have developed.

The most abundant mechanical energy is that from human motion in our daily life. Wearable electronics is increasingly needed for various applications such as clothes, eye glasses, wristwatches. Recently, there have been many attempts to fabricate wearable electronics using piezoelectric and triboelectric. Actually fiber-based piezoelectric generator for wearable electronics and mobile medication is already demonstrated. Also, woven structured triboelectric nanogenerator for wearable device is developed.

The emerging technologies for such mechanical energy harvesting have been proven to be effective and promising approaches for building self-powered systems. In particular, it is highly desired for implanted biomedical devices to be self-powered without using a battery. Various mechanical energies such as heart beat and muscle stretching exist in human body enough to power the implanted devices to build nanosystems. Actually, in vivo biomechanical-energy harvesting from mechanical energies such as the muscle movement and heart beat in a live rat was already demonstrated [14]. Implantable energy harvester by periodic breathing and a self-powered artificial pacemaker using living heart in human body was also developed [15].

Recently, many researchers have taken key advances toward practical uses of biocompatible electronic devices that could be implanted into the body, in which the electronic devices are operated steadily without pain for a specific period of time, and then dissolve harmlessly when no

ULSAN NATIONAL INSTITUTE OF SCIENCE AND TECHNOLOGY

longer needed without requiring an extra surgery to remove them from the body. Thus, it is essential to explore innovative technologies for developing the time-controllable biodegradable nanogenerator to power such implanted electronic devices. Until now, polydimethylsiloxane (PDMS) elastomer was widely used as the supporting polymer in composite-type nanogenerators due to its high shear strength, low Young's modulus, and flexibility. But, surface of PDMS is too sticky and easily adhesive to various material surface due to Van der Waals forces.

Here, we replace the PDMS to the silk fibroin, producing silk fibroin-based composite-type nanogenerators with biocompatible ferroelectric nanoparticles. Silk fibroin is a natural polymer with biocompatible, transparent and biodegradable properties (soluble in water), which has been used as platforms for transistors and various classes of photonic devices. Furthermore, it shows excellent mechanical properties (tensile strength ~ 100 MPa), expecting good durability and the application under various external stress [17]. Additionally, the unique time-controllable property of silk fibroin composite was demonstrated and is so desirable for operation of biocompatible nanogenerator in human skin and body.

And we also reported the textile structured triboelectric nanogenerator by integrating and connecting several PDMS tube structured triboelectric nanogenerators in parallel for wearable devices. PDMS and Au were chosen as the triboelectric materials because of the large difference in their ability to lose and gain electrons in triboelectric series. Firstly we made tube- and cable structured triboelectric nanogenerator consisting of Au wire and PDMS tube having nano-patterned surface. We investigated the relationships between the diameter of tube and output performance. Also we showed the change of output performance of applied stretching. At last, the textile structured triboelectric nanogenerator is applied in wearable devices to harvest different kinds of mechanical energies in human body.-

ULSAN NATIONAL INSTITUTE OF SCIENCE AND TECHNOLOGY

II. Experimental Method

2.1 Preparation of silk fibroin solution

The silk fibroin solution here was prepared from Bombyx mori cocoons and was described previously [18-20]. Roughly, the cocoons were boiled for 20 min in a solution of 0.02 M sodium carbonate (Na_2CO_3) to remove the sericin protein. The extracted fibroin was rinsed with distilled water (DI) and then dried in ambient air for 12 hrs. After drying, the fibroin was dissolved in a 9.3 M lithium bromide (LiBr) solution at 60^{o}C for 4 hrs, yielding a 20 wt% aqueous solution. Subsequently, the solution was dialyzed against the DI water using a dialysis cassette (Slide-a-Lyzer, Pierce, MWCO 3.5K) at room temperature for 48 hrs until the solution reached a concentration of 8 wt%. The obtained solution was purified using a centrifuge and a 0.8 mm syringe filter.

2.2 Preparations of $BaTiO_3$, $ZnSnO_3$, BNKT, KNN:Mn, nanoparticles

BaTiO3 (99.9%) nanoparticles were supplied by US Research Nanomaterials, Inc. The synthesis of the other nanoparticles is shown in Figure 1.

$ZnSnO_3$ nanoparticles were prepared by an aqueous solution method.10 mmol $ZnSO_4$-$7H_2O$ was added to 100 ml DI water and was stirred until the nanoparticles were dissolved completely. The Na_2SnO_3-$3H_2O$ was then poured into the solution, resulting in a 1:1 molar ratio of zinc and tin precursors. The solution was violently stirred at 80^{o}C during 5 hrs. After that the products are rinsed with distilled water 5 times and dried in the oven at 90^{o}C for 1 hr [11].

$Bi_{0.5}(Na_{0.82}K_{0.18})_{0.5}TiO_3$ (BNKT) and $K_{0.5}Na_{0.5}Nb_{0.995}Mn_{0.005}O_3$ (KNN:Mn) nanoparticles were synthesized by heat treatment of chemical solutions which were prepared by sol-gel method. Bismuth nitrate pentahydrate, sodium nitrate, potassium nitrate, and titanium butoxide were used as precursors for BNKT sol [21]. Potassium nitrate, sodium nitrate, niobium pentaethoxide, and manganese acetate were used as precursors for KNN:Mn sol [22]. Acetic acid and 2-methoxyethanol were used as solvent. Acetylacetone was used as complexing agent to stabilize of alkoxide precursors. The chemical solutions were dried at 120 ^{o}C for 24 hrs, followed by heating at 400 ^{o}C for about 5 hrs to expel trace amounts of water and carbon. Then the products were calcined at 650~800 ^{o}C.

ULSAN NATIONAL INSTITUTE OF SCIENCE AND TECHNOLOGY

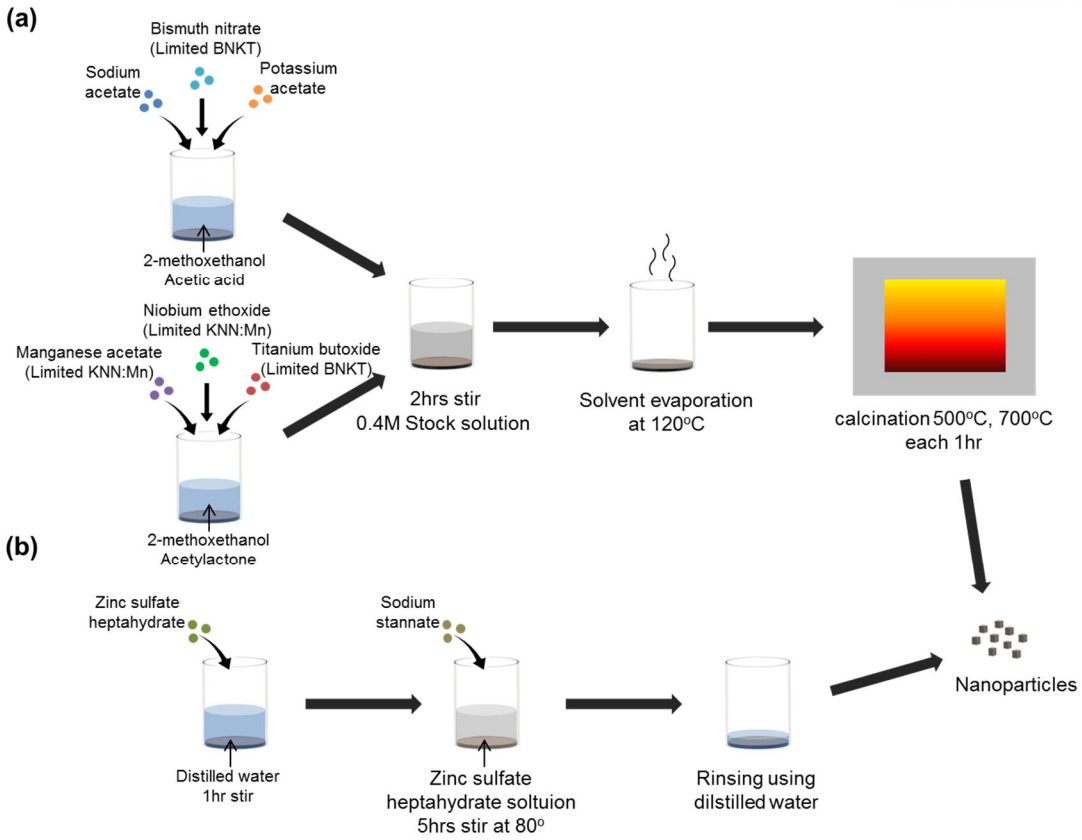

Figure 1 Synthesis of (a) BNKT, KNN:Mn and (b) $ZnSnO_3$ ferroelectric nanoparticles.

ULSAN NATIONAL INSTITUTE OF SCIENCE AND TECHNOLOGY

2.3 Fabrication of silk fibroin based composite nanogenerator

0.0125 g polyvinylpyrrolidone (PVP) was initially mixed in 0.5 g Ag nanowires (Nanotech and Beyond co., Ltd.), poured into the silk solution. The nanoparticles (BNKT, KNN:Mn, $BaTiO_3$, $ZnSnO_3$) are then added to the solution, producing the 30 wt% silk composite solution. The well-mixed solution was spin-coated onto the ITO/PET flexible substrate, and cured at room temperature for 1 day. Glycerol was used to control the biodegradable properties of the silk fibroin film. The other ITO/PET film was attached onto the composite layer, acting as the top electrodes. The Cu wires were attached to both electrodes by means of Ag paste for the measurement of the output voltage and current density.

2.4 Fabrication of the tube structured triboelectric nanogenerator

The source materials for the tube structured triboelectric nanogenerator are PDMS, aluminum wire and foil. The fabrication of the tube structured triboelectric nanogenerator is shown in Figure 1a. The PDMS tube is fabricated by coating a 10:1 ratio (v:v) mixture of Sylgard 184 elastomer and Sylgard 184 elastomer curing agent on aluminum wire with various diameters. And PDMS coated aluminum wire is dried at 90 ^{o}C in oven for 20 min, and are immersed in acetone for 20 min. And then PDMS tube is peeled-off from the aluminum wire as single continuous products. The PDMS tube is cut in half along its length and decorated by coating 100 nm sized Au nanoparticles at a concentration of 56.6 mg/l (BBI solutions). And then the RIE process was performed with 37 sccm CF_4 and 13 sccm O_2 mixtures at 270 W for 20 min. The etched nanowire is uniformly distributed on the inner surface of the PDMS tube which has an average length of 1 μm and diameters ranging from 80 to 125 nm. The precursor solution of ZnO was deposited onto Al wires by dip coating, the wires were dried at 500 ^{o}C. The dried samples are loaded into Teflon-sealed stainless autoclave and were put facing down on the nutrient growth solution (1:1 ratio of zinc nitrate and hexamethylenetetramine (HMTA) 20 mM) and were kept in an oven at 90°C for 3 hrs. And then the samples were loaded into an e-beam evaporator to form Au electrode. Au (100 nm thickness) layer was evaporated using high purity Au at a base pressure 3.0 x 10^{-6} Torr and room temperature. The deposition rate was fixed to be approximately 1 nm s^{-1}. The voltage was set to be 6 kV. The Al foils were wound around the nanostructured PDMS tubes to form electrodes, and Au coated wires were placed inside the nanostructured PDMS tube. And then, the fabricated tube structured triboelectric nanogenerator was then sealed with PDMS so that it is fully waterproof from the humid environment.

ULSAN NATIONAL INSTITUTE OF
SCIENCE AND TECHNOLOGY

2.5 Fabrication of the cable and textile structured triboelectric nanogenerator

The aluminum wire of length 30 cm having a diameter of 0.6 mm is prepared to fabricate textile triboelectric nanogenerator and performed by same method with above experiment. The three tube triboelectric nanogenerators are tied into groups of ten using normal PDMS and are woven a piece of textile.

2.6 Microstructural analysis

The morphologies of the synthesized ferroelectric composite and the morphologies of the PDMS and Au pattern arrays were characterized by a Nano 230 field emission scanning electron microscope (FEI, USA). The crystalline properties of the films were characterized by a high resolution X-ray diffractometer (Bruker, Germany).

2.7 Measurement system

I-V characteristics with the applied force were obtained under an air ambient using a Keithley 2636A source measurement unit. To measure the current densities and voltages generated by piezoelectric silk fibroin composites, a Keithley 6485 picoammeter and Keithley 2182A voltammeter were used.

And we measured the output voltages of the textile structured triboelectric nanogenerators by applying a pushing force. A pushing tester (Labworks Inc., model no. ET-126-4) was used to create a vertical compressive strain in the triboelectric nanogenerator. To detect currents and voltages generated by textile structured triboelectric nanogenerator, an oscilloscope (Agilent technology Inc., model no. DSO1024a) and a low-noise current preamplifier (Stanford research systems Inc., model no. SR570) was used.

ULSAN NATIONAL INSTITUTE OF SCIENCE AND TECHNOLOGY

III. Results and Discussions

3.1 Silk fibroin based biodegradable and piezoelectric composite nanogenerator

3.1.1 Fabrication of silk based nanogenerator

The schematic diagrams of the fabrication process are shown in Figure 3a and detail information described in Experimental section and Figure 2.

Figure 3b shows the cross-sectional scanning electron microscopy (SEM) image of the KNN:Mn nanoparticles and the crystallographic structure of the material in the inset, exhibiting a well-defined cubic morphology with an average size of about 400 ~ 500 nm. The pristine silk film and silk composite film are seen to have a uniform thickness of about 15 ~ 20 μm, as shown in Figures 3c and 3d. In Figure 3e, a High magnification SEM image of composite film is shown. It was clearly seen that the nanoparticles are seen to be well-dispersed in the silk matrix. $BaTiO_3$, $ZnSnO_3$, and BNKT nanoparticles with same size distribution are also prepared and the SEM images of the composites embedded with the nanoparticles are seen in Figure 4.

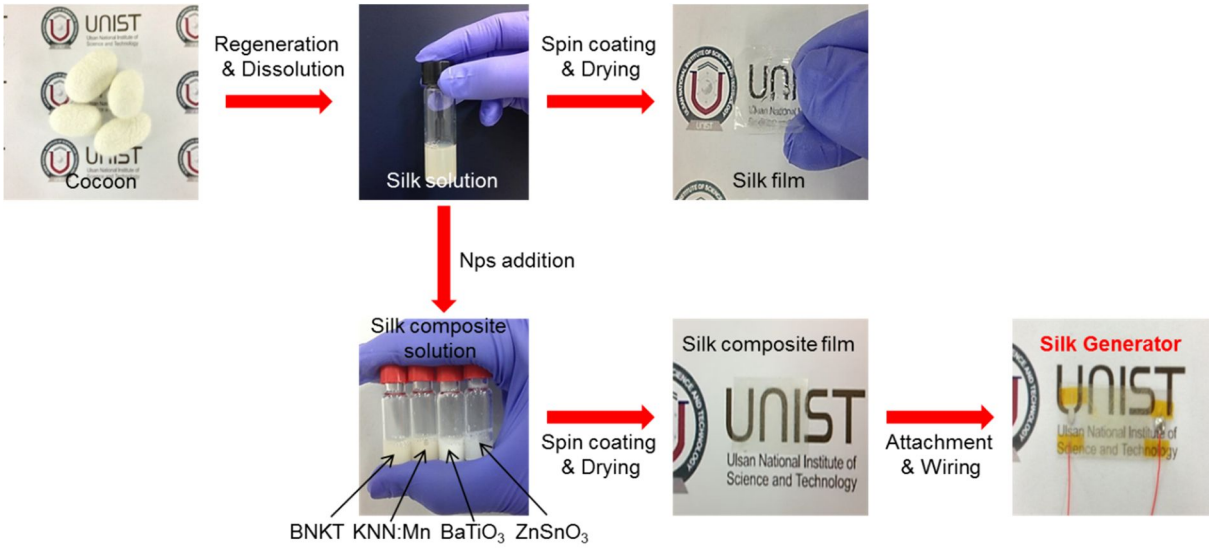

Figure 2 Fabrication process of silk fibroin film and silk fibroin-based composite-type generators.

ULSAN NATIONAL INSTITUTE OF SCIENCE AND TECHNOLOGY

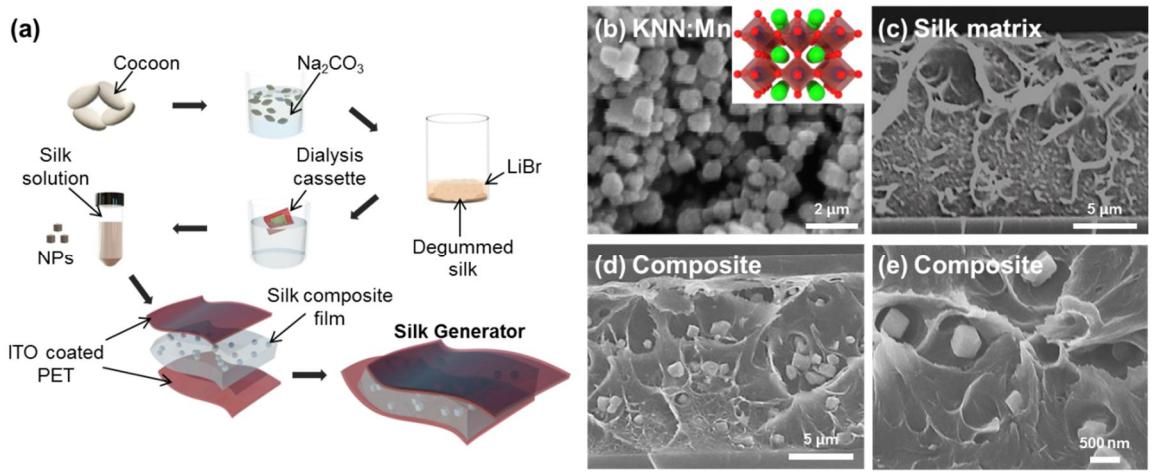

Figure 3 (a) Schematic diagrams of the fabrication process for the silk fibroin-based composite-type nanogenerators with ferroelectric particles. (b) A SEM images of Mn doped KNN nanoparticles with an edge size of about 400-500 nm. The inset shows the crystallographic structure of Mn doped KNN, showing orthorhombic structure. A cross-sectional SEM photograph of (c) a silk fibroin matrix and (d) a composite film. (e) A High magnification SEM images of composite film.

ULSAN NATIONAL INSTITUTE OF
SCIENCE AND TECHNOLOGY

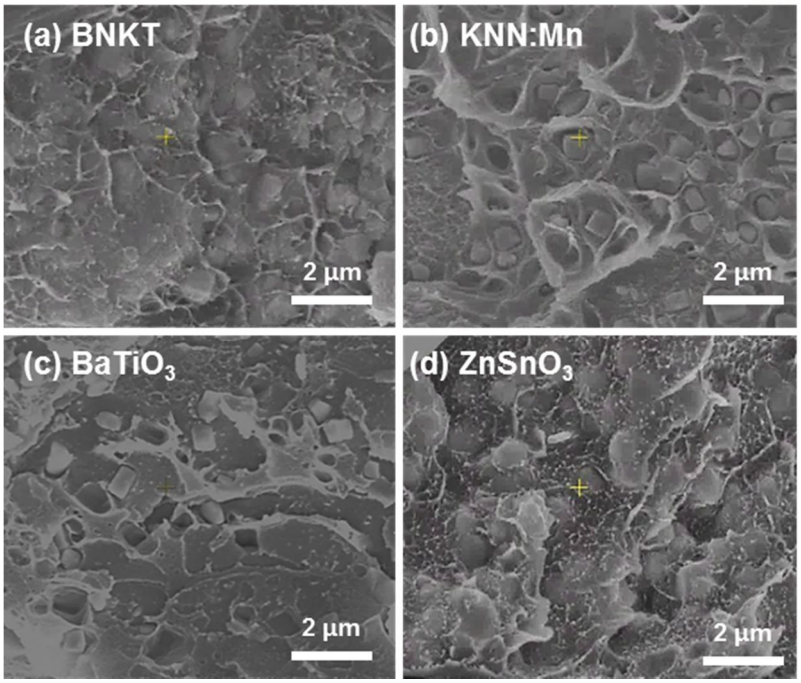

Figure 4 The high magnification cross-sectional SEM images of (a) BNKT, (b) KNN:Mn, (c) $BaTiO_3$ and (d) $ZnSnO_3$ composite films

ULSAN NATIONAL INSTITUTE OF SCIENCE AND TECHNOLOGY

3.1.2 Various property of silk based nanogenerator

Figure 5a shows high resolution X-ray diffractometer (XRD) profiles of pure silk fibroin film and composite films with 30 wt% $BaTiO_3$, $ZnSnO_3$, BNKT, and KNN:Mn nanoparticles. The pure silk fibroin film shows an XRD pattern of typical amorphous material, with the absence of crystallinity peaks, characterizing a silk I secondary structure which mainly consists of α-helix and random coil. For the composite films, it is clearly seen that the nanoparticles are fully crystallized, and no impure phases are observed in the samples. The crystal structures of the $BaTiO_3$, $ZnSnO_3$, BNKT, and KNN:Mn nanoparticles are indexed to the tetragonal, rhombohedral, rhombohedral-tetragonal morphotropic phase boundary (MPB), orthorhombic structures. The electrical properties of the films along the vertical direction were examined, showing that the films provide excellent insulating properties although the composites show a little increase in the conductivity, as shown in the inset of Figure 5b. The optical transmittance of the films are measured and plotted in Figure 5c. The 15 μm-thick silk fibroin film on ITO/PET substrate show a transmittance of about 85 % in the range of 400 to 800 nm. As the 30 wt% KNN:Mn nanoparticles are added to the silk fibroin solution, the transmittance decreases up to 72 %, in which the decrease in the transmittance is irrespective of the nanoparticles. The composite films are still seen to be quite transparent, as shown in Figure 5c.

ULSAN NATIONAL INSTITUTE OF SCIENCE AND TECHNOLOGY

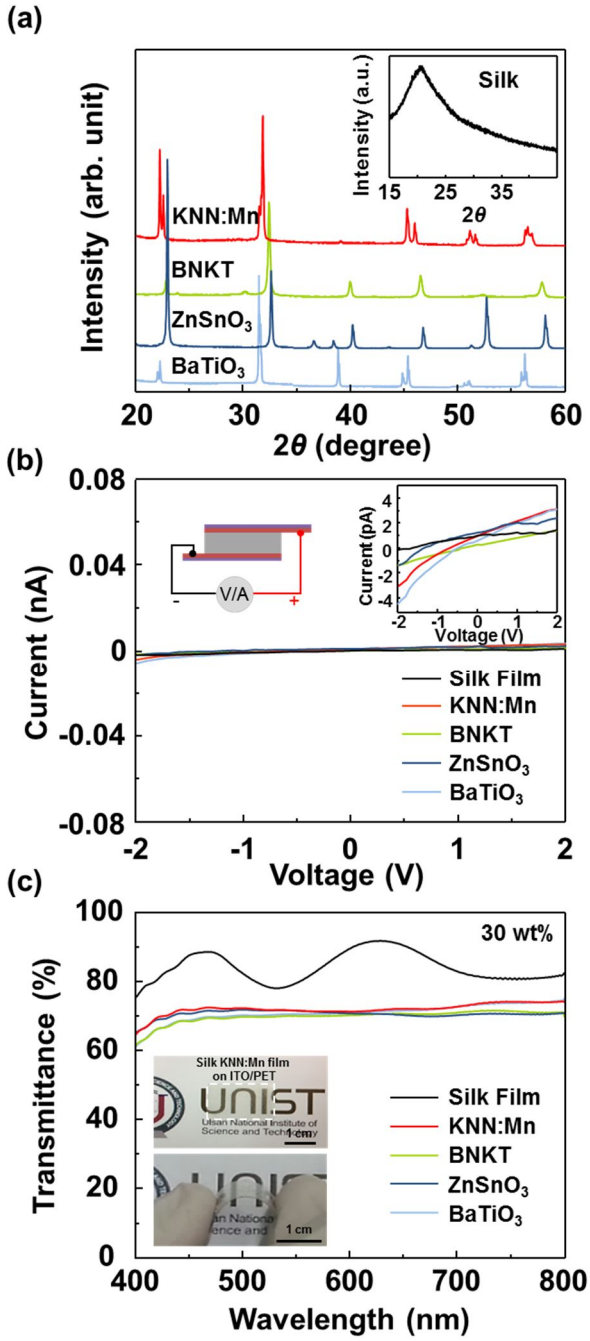

Figure 5 (a) XRD profiles of the composite films with 30 wt% BaTiO3, ZnSnO3, BNKT, and KNN:Mn nanoparticles. The inset is the XRD profile of pure silk fibroin film. (b) The current-voltage (I–V) characteristic of the silk fibroin film and composite films along the vertical direction. The inset graph enlarges up the films. (c) The transmittance spectrum as a function of wavelength of silk fibroin film and composite films that indicates the high transparency of the composite films. The top inset shows the photographs of flexible and transparent silk fibroin-based composite-type films contained Mn doped KNN nanoparticles on ITO/PET substrate, and bottom inset shows the flexibility of composite films by bending with fingers.

ULSAN NATIONAL INSTITUTE OF SCIENCE AND TECHNOLOGY

3.1.3 Output performance of silk based nanogenerator

The composite with 50 wt% nanoparticles still shows a transmittance of approximately 65 % (Figure 6a).

To measure the piezoelectric power-generating performance of the device, a direct impact approach was used. A foot of human was used to apply vertical compressive force on the devices. Figures 8a and 8b show a photography of the actual experimental setup for scavenging energy from the foot motion, and the output voltage and current density generated from the composite film type nanogenerator with 30 wt% KNN:Mn nanoparticles, respectively. It was clearly seen that an output voltage of 2.2 V and a current density of 0.12 $\mu A/cm^2$ were obtained by the normal pushing force. This power-generation performance was quite stable. Further increases in the concentration to 50 wt% decreases the output power, due to the weakness of insulation resulting to the electric breakdown (see Figure 6b). Polarity-switching tests also confirm that the output voltage and current density originated from the piezoelectric phenomenon (Figure 6c). Figure 7 also shows the change of calculated piezopotentials of the composite nanogenerator with the magnitude of applied force. It can be clearly seen that the change of the piezopotentials increased linearly as the external force increased from 100 to 500 μN for the composite film type nanogenerator.

ULSAN NATIONAL INSTITUTE OF SCIENCE AND TECHNOLOGY

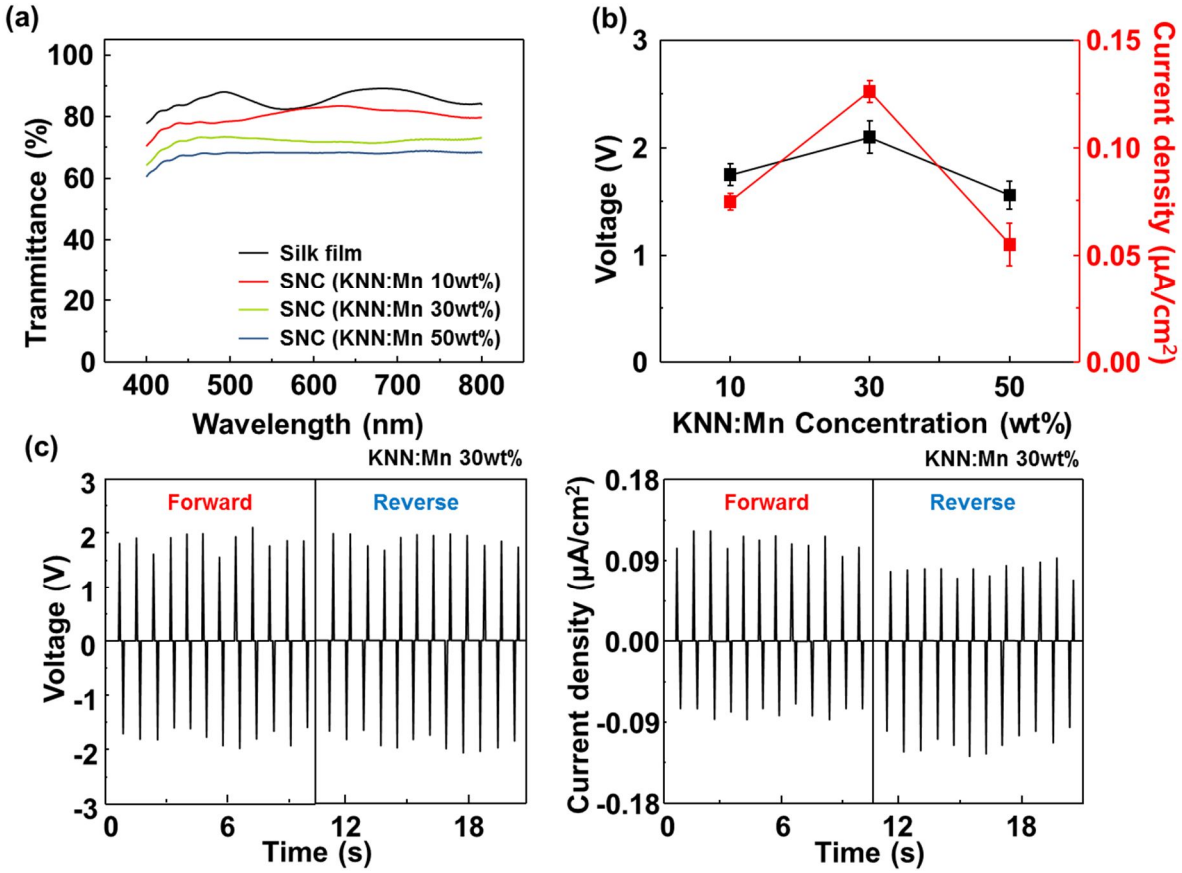

Figure 6 (a) The transmittances and (b) output voltages and current densities of silk fibroin-based composite-type film in the various concentrations of KNN:Mn nanoparticles. (c) Polarity-switching test of silk fibroin-based composite-type generator.

ULSAN NATIONAL INSTITUTE OF
SCIENCE AND TECHNOLOGY

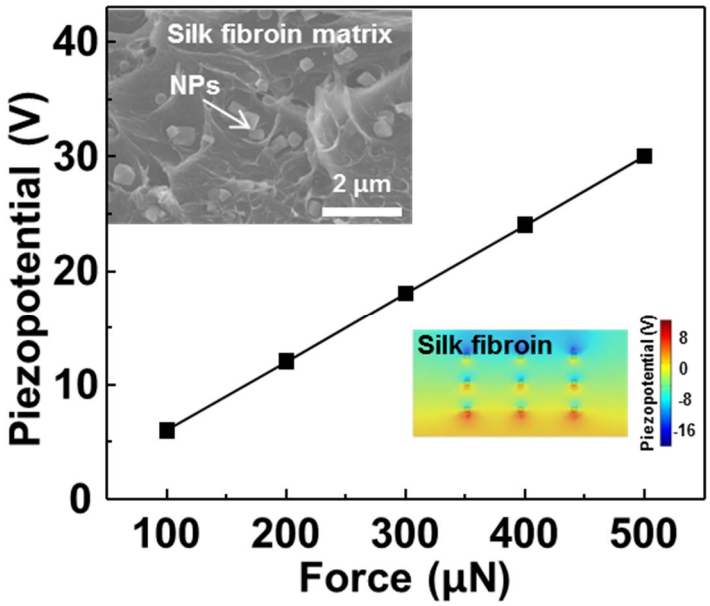

Figure 7 The piezopotential from theoretical model of the silk fibroin-based composite-type generator as a function of force. And the top and bottom inset shows the SEM images of silk fibroin-based composite-type film and the piezopotential distribution.

ULSAN NATIONAL INSTITUTE OF SCIENCE AND TECHNOLOGY

As mentioned above, we believe that the nanoparticles with same size distribution (400 ~ 500 nm) are well-dispersed in the silk fibroin matrix. However, it may not be easy to investigate how the nanoparticles are dispersed in the matrix. Furthermore, the silk fibroin solution is so low viscous that the nanoparticles naturally and easily sink into the surface of the substrate, as shown in the left inset of Figure 8c. As expected, the composite nanogenerator with poor dispersion generates the low output voltage of less than 1 V in Figure 8c. To enhance the dispersion, Ag nanowires and PVP were used as dispersing agents and the optimization process was used to promote the dispersed distribution. It is well-known that the Ag nanowires are widely used in dispersing the nanoparticles in the composites, and developing the transparent and conducting electrodes [23-25]. Thus, the PVP was added to the solution to reduce the conductivity of the films (see the inset of Figure 8d), thereby, increase the output performance of the nanogenerator. Actually, when the nanoparticles are mixed into the silk fibroin solution with Ag nanowires (1 wt%) and PVP (12 wt%) together, a maximum output voltage and current density of 2.2 V and 0.12 $\mu A/cm^2$ were obtained, 2 times higher than that for only KNN:Mn nanoparticles in Figures 8c and 8d. It is thought that the PVP plays role in dispersing nanoparticles in the silk fibroin matrix and wrapping a surface of Ag nanowires in order to prevent Ag nanowires from connecting with each other [26]. The cross-sectional image in the right inset of the Figure 8c confirms that the nanoparticles are well-dispersed in the silk fibroin matrix. In the Figure 9, the calculated piezopotential difference between of aggregated and well-dispersed nanoparticles in the silk fibroin matrix is in good agreement with experimental results.

ULSAN NATIONAL INSTITUTE OF SCIENCE AND TECHNOLOGY

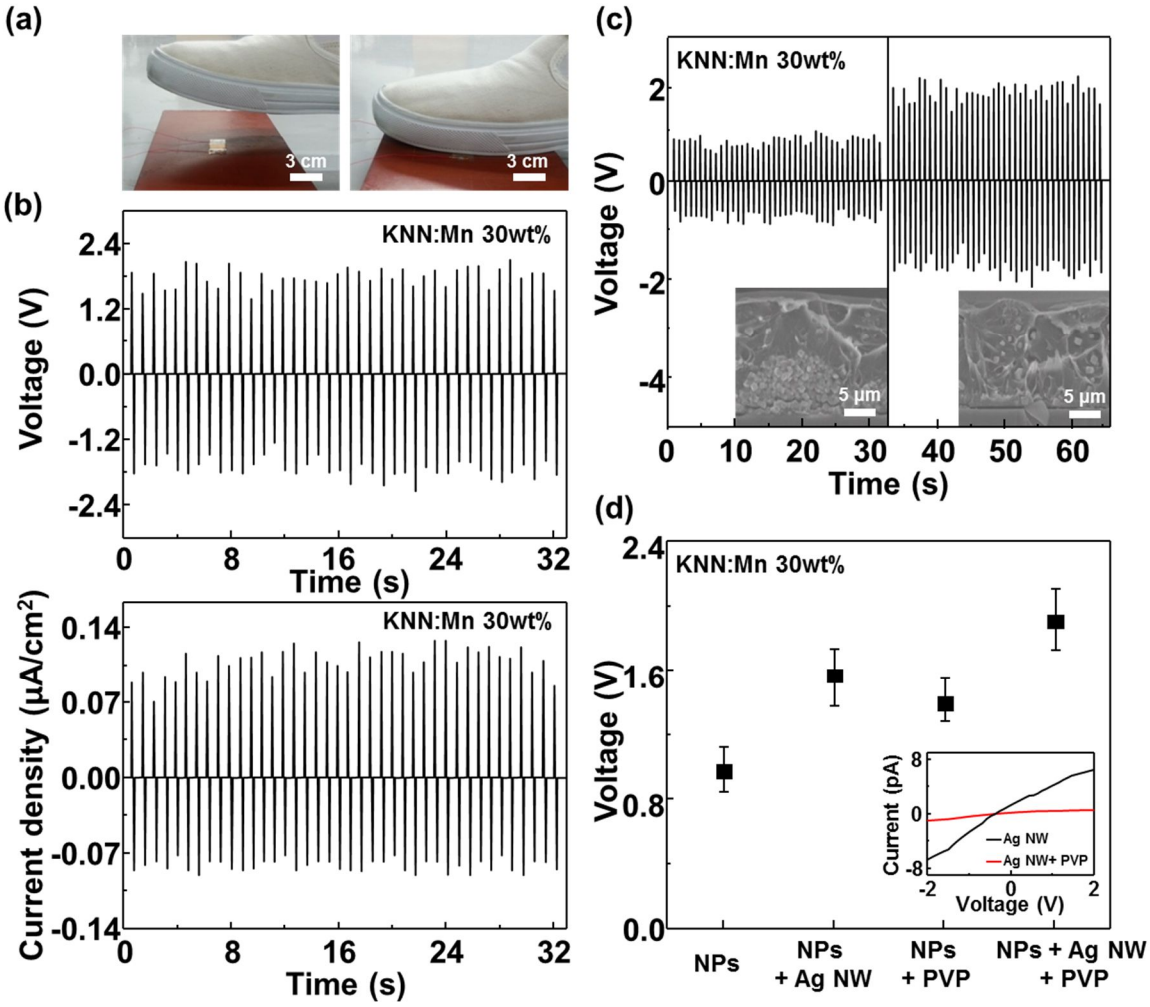

Figure 8 (a) The original images indicating the experimental setup for power generation under the foot step in which silk fibroin-based composite-type generator was laid down a woodblock. (b) The output voltage and current density generated from the composite film type nanogenerator with 30 wt% KNN:Mn nanoparticles. (c) The output voltage generated from the devices fabricated using KNN:Mn NPs without and with dispersants in the silk fibroin matrix. The inset indicates the magnified cross-sectional SEM image of the aggregation of the NPs and the well-dispersed NPs. (d) The generated output voltages of the devices fabricated using the different combination of dispersant. The inset shows the current-voltage (I–V) characteristic of only Ag nanowires and Ag nanowires-PVPs composite in the silk matrix films along the vertical direction to identify PVP effect.

ULSAN NATIONAL INSTITUTE OF SCIENCE AND TECHNOLOGY

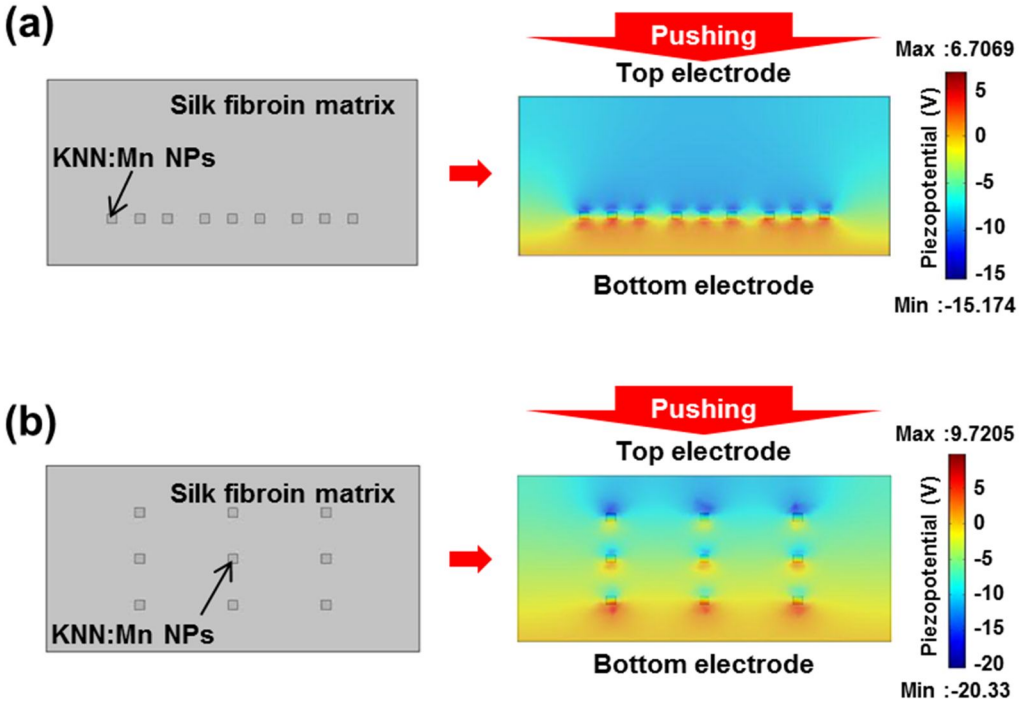

Figure 9 The calculated piezopotential difference between of (a) aggregated and (b) well-distributed ferroelectric particles in the silk fibroin matrix.

ULSAN NATIONAL INSTITUTE OF SCIENCE AND TECHNOLOGY

The output power of the composite nanogenerator is also dependent on the piezoelectric coupling figure of merit, which is defined as k^2Q. Here, k is a measure of the conversion efficiency between electrical and mechanical energy in piezoelectric materials and Q indicates the quality factor of the device. The maximum power generated is obtained in the generator with a high k and Q-factor when the generator works at its resonant frequency. It may be generally acceptable that Mn doping can significantly enhance the mechanical quality factor without deteriorating other piezoelectric properties, expecting the large Q-factor in composites embedded with KNN:Mn nanoparticles (the Q-factor of the composites embedded with various nanoparticles will be separate paper) [27-29]. The electromechanical coupling factor (k) can be expressed by

$$k^2 = Y \times d_{ij}^2 / \varepsilon^2$$

where Y, d_{ij}, and ε^T are Young's modulus, piezoelectric coefficient, and dielectric constant, respectively [30-31]. Nanoindentation measurements were conducted to evaluate the resistance to deformation by external force, and show that there is no significant change in the elastic modulus (0.2 ~ 0.3 GPa) in composites. We also believe that the Ag nanowires do not affect the dielectric properties of the silk fibroin materials because of the low volume fraction (as low as 7 %) [26]. Thus, it is essential in increasing the piezoelectric constant (d_{ij}) for the larger output power of the nanogenerator. In Figure 10, among the nanoparticles ($BaTiO_3$, $ZnSnO_3$, BNKT, and KNN:Mn), the KNN:Mn has the largest piezoelectric coefficient (d_{33}) of ~ 270 pC/N and relatively small dielectric constant of about 730 [32]. Thus, the coupling factor of the material is expected to be the highest, leading to the largest output power, consistent with experimental results.

ULSAN NATIONAL INSTITUTE OF
SCIENCE AND TECHNOLOGY

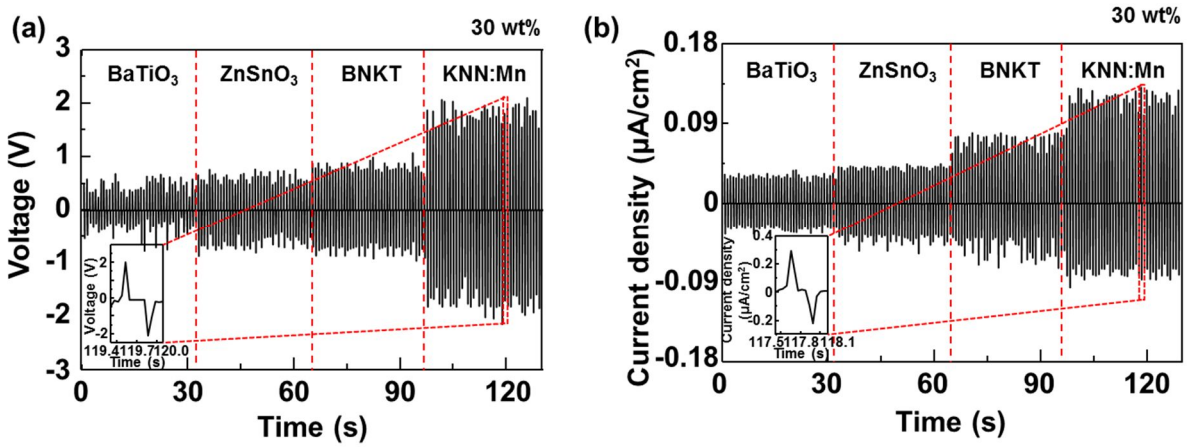

Figure 10 (a) The output voltages and (b) current densities of the various ferroelectric particles when the concentrations of ferroelectric particles are 30 wt%. The insets illustrate the enlarged graphs of the output signals from the boxed areas

ULSAN NATIONAL INSTITUTE OF SCIENCE AND TECHNOLOGY

3.1.4 Biodegradable property of silk based nanogenerator

The composite films formed from the silk fibroin and the nanoparticles are soluble in water because of the random coil structures, which make the composites generator useless within 10 min. This may be quite meaningful when the powering devices need to disappear with the implanted electronic devices when no longer needed. But, it is essential to develop the nanogenerators that can disappear in a controlled and programmable way. For example, the medical implants, that are needed for a few weeks and then disappear, may need the nanogenerators powering to the implanted devices during the same periods, without requiring an extra surgery to remove them from the body. Glycerol has been used to control the biodegradable properties of the silk fibroin film. That is, it is able to accelerate silk gelation, making the silk fibroin film insoluble in water due to high content of β-sheet. When the glycerol content in the blend films increases to 5 wt%, the composite films are completely dissolved after dipping in the water for 30 min. Further increases in glycerol to 20 wt% and more concentrations significantly reduced the solubility up to 48 hrs, as shown in the inset of the Figure 11a, and there is no significant change in the output voltage of the composite nanogenerators, as shown in Figure 11c. The result indicates that 20 wt% glycerol was a critical concentration in inducing the structural transition from random coil to β-sheet which is water-insoluble [33]. This results show that it is possible to disappear the composite films in a controlled way for transient electronics.

ULSAN NATIONAL INSTITUTE OF
SCIENCE AND TECHNOLOGY

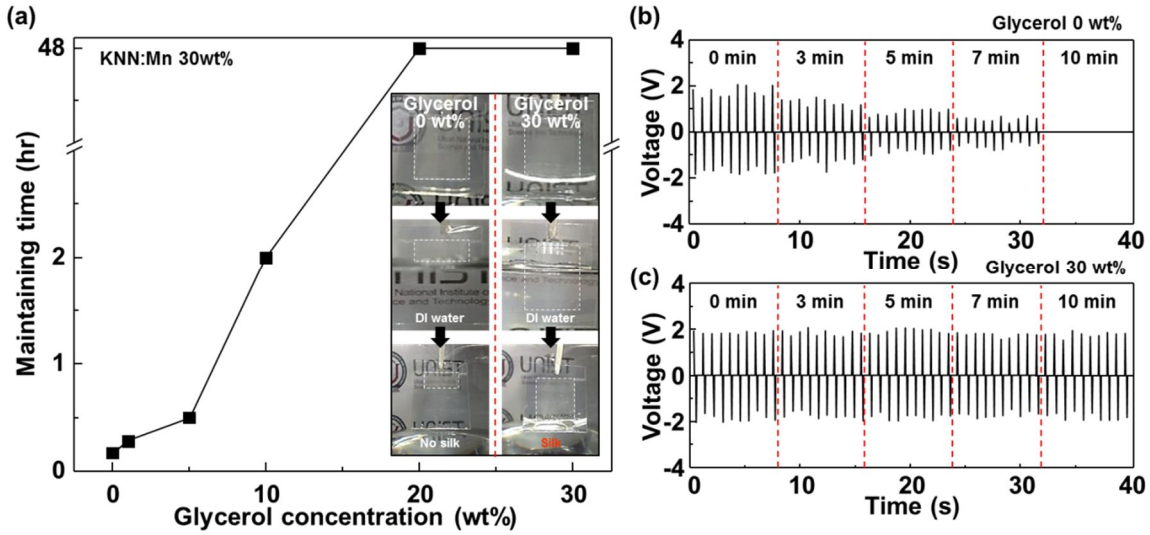

Figure 11 (a) The maintenance time of composite film fabricated with various glycerol concentrations. The left inset shows the photograph of dissolution of the pure silk fibroin film on ITO/PET substrate in distilled water, and the right inset shows the image of insolubility of the film for the compositions of 30wt% glycerol embedded silk fibroin film. The immersion time-dependent change output voltage for (b) the pure silk fibroin-based composite-type film and (c) 30wt% glycerol blend film.

ULSAN NATIONAL INSTITUTE OF
SCIENCE AND TECHNOLOGY

3.1.5 One-dimesional wire nanogenerator

A nanogenerator was also made as a form of a one-dimensional (1D) wire, and the output power was measured in a same fashion. It was done by dip-coating silk fibroin-based composite-type solution onto an aluminum wire and composite layer is cured at 50°C. Then semi-cured composite wire was taped with Al foils as electrode. In Figures 12a and 12b, The wire consists of Al wire (diameter 1 mm) at the inner, silk fibroin composite (~20 μm), and Al sheet (~ 20 μm) at the outer. The nanogenerator shows the output voltage of ~ 1.8 V and the output current density of ~ 0.1 $\mu A/cm^2$ in Figure 12c, showing a similar output performance of thin film type nanogenerator, as shown in Figure 9. This will provide the feasibility of this 1D wire as a promising path toward the development of a robust textile nanogenerator for the future smart clothing industry.

ULSAN NATIONAL INSTITUTE OF
SCIENCE AND TECHNOLOGY

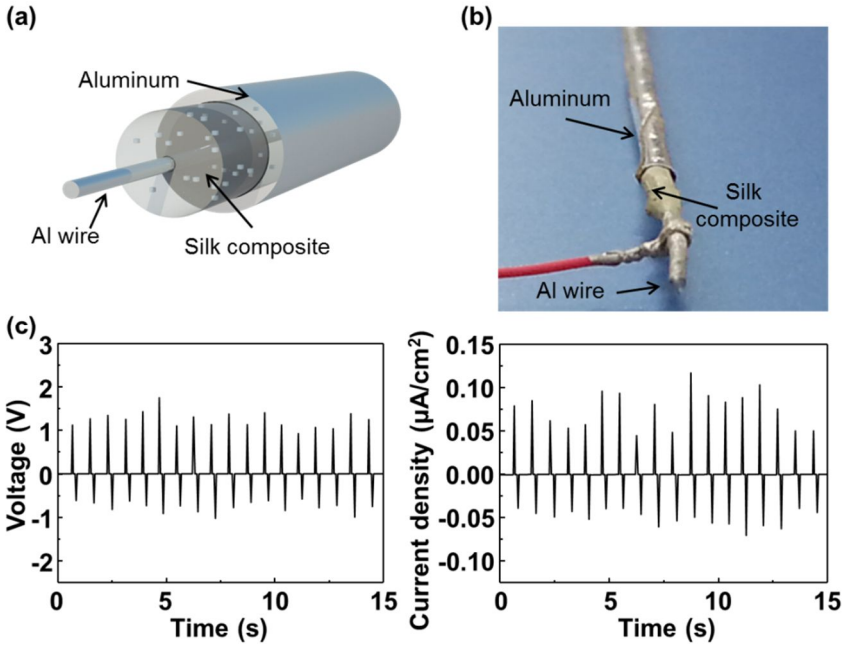

Figure 12 (a) A schematic image and (b) a photograph of silk fibroin-based composite-type wire generator which consists of Al wire, silk fibroin composite layer and aluminum electrode. (c) The output voltage and current density of silk fibroin-based composite-type wire generator.

ULSAN NATIONAL INSTITUTE OF SCIENCE AND TECHNOLOGY

3.2 Textile structured triboelectric nanogenerator for wearable electronics

3.2.1 Fabrication of tube structured triboelectric nanogenerator

The schematic diagrams of the fabrication process are shown in Figure 13a and detail information described in Experimental section. Figure 13b shows the cross-sectional scanning electron microscopy (SEM) image of the Au coated aluminum nanowire and PDMS nanowire. The Au coated aluminum wires are seen to have a uniform length of about 0.8 ~ 1 μm and diameter of about 100 nm. Figure 13c shows the output voltage and current generated from the tube structured triboelectric nanogenerator. It was clearly seen that an output voltage of 40 V and a current 10 μA were obtained by the normal pushing force. And then, this power-generation performance was quite stable. The electrical output performance of the tube structured triboelectric nanogenerator and sealed tube structured triboelectric nanogenerator were measured and plotted under 95 % relative humidity conditions, as shown in Figure 13d. The tubes have diameters of 5 mm as shown in inset of Figure 13d. In case of tube structured triboelectric nanogenerator without sealing, the output performance decreases to its original level when relative humidity increases to 95 %. While the sealing treatment using PDMS will isolate the nanogenerator from the humid environment, resulting in a constant power output from the beginning.

ULSAN NATIONAL INSTITUTE OF SCIENCE AND TECHNOLOGY

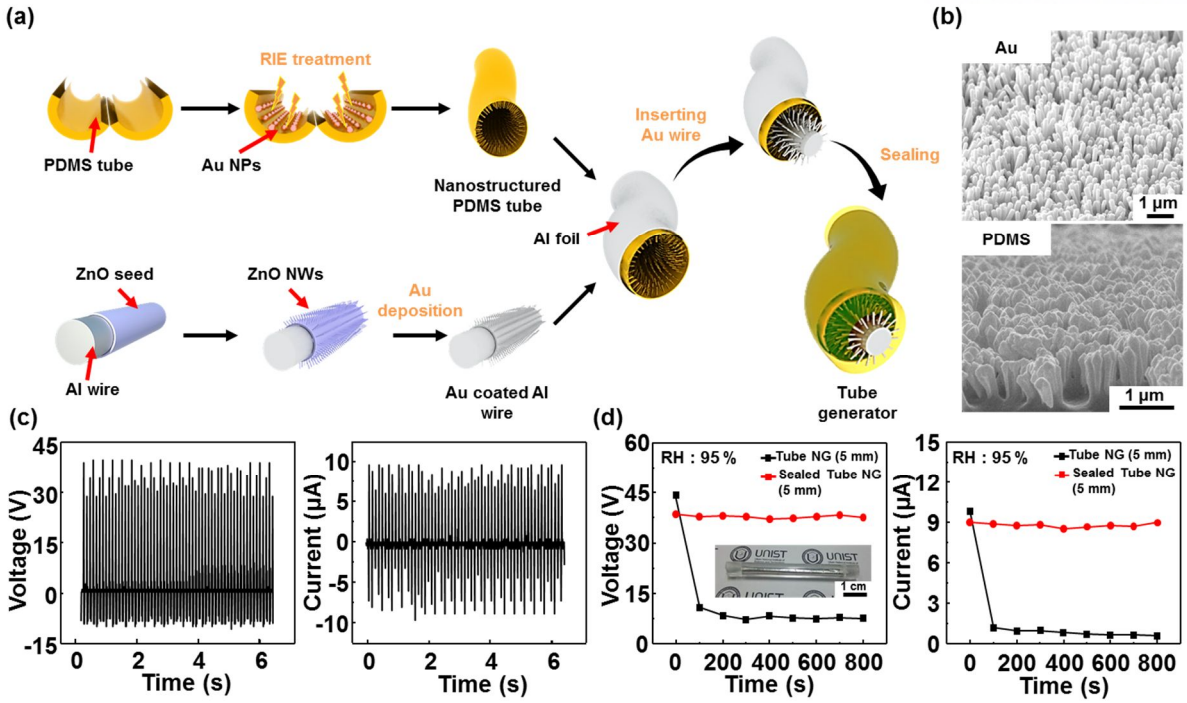

Figure 13 (a) The fabrication of tube structured triboelectic generator. (b) The SEM image of nanostructured Au coated Al wire and PDMS (c) The output performance of tube structured triboelectric generator with 7 mm diameter of tube. (d) The sealing effect of tube structured triboelectric generator

ULSAN NATIONAL INSTITUTE OF
SCIENCE AND TECHNOLOGY

The mechanism of tube structured triboelectric generator can be expressed by the coupling effect between triboelectrification and electrostatic induction in Figure 14. At the original state, the PDMS tube and the Au wire is fully separated by sealing treatment using PDMS as indicated in Figure 14a, and there is no charge transfer. The PDMS tube is in fully contact with the Au wire when the external impact is applied. In the Figure 14b, the triboelectric charges which are negative charges on the PDMS and positive charges on the Au wire are produced at the contact surfaces, because electrons are injected from the Au wire to the PDMS tube due to large difference in triboelectric series. There are no flows in the circuit, because of the contact electrification process that is the generated charges with opposite polarities are totally offset. When the external impact is receded, a relative separation between the Au wire and the PDMS tube is happened. The negative charges and the positive charges can't be compensated. As a result, the positive charges are induced on the Al electrode attached onto the PDMS tube, and free electrons flow from the Al electrode to the Au wires through the external circuit (Figure 14c). As the tube structured triboelectric nanogenerator reverts back to the original position, the negative charges on the PDMS tube can be fully screened, inducing an equal amount charges on the Al electrodes as sketched in Figure 14d. Subsequently, the external impact is applied once again, the PDMS tube is reverted to the Au wires. The induction of positive triboelectric charges on the Al electrode decreases. Consequently, the free electrons flow in a reversed direction from the Au wire to Al electrode in order to eliminate the difference of electric potential (Figure 14e). The PDMS tube and Au wire fully contact each other and complete a whole process of triboelectricity generation denoted as the coupling effect between triboelectrification and electrostatic induction.

ULSAN NATIONAL INSTITUTE OF SCIENCE AND TECHNOLOGY

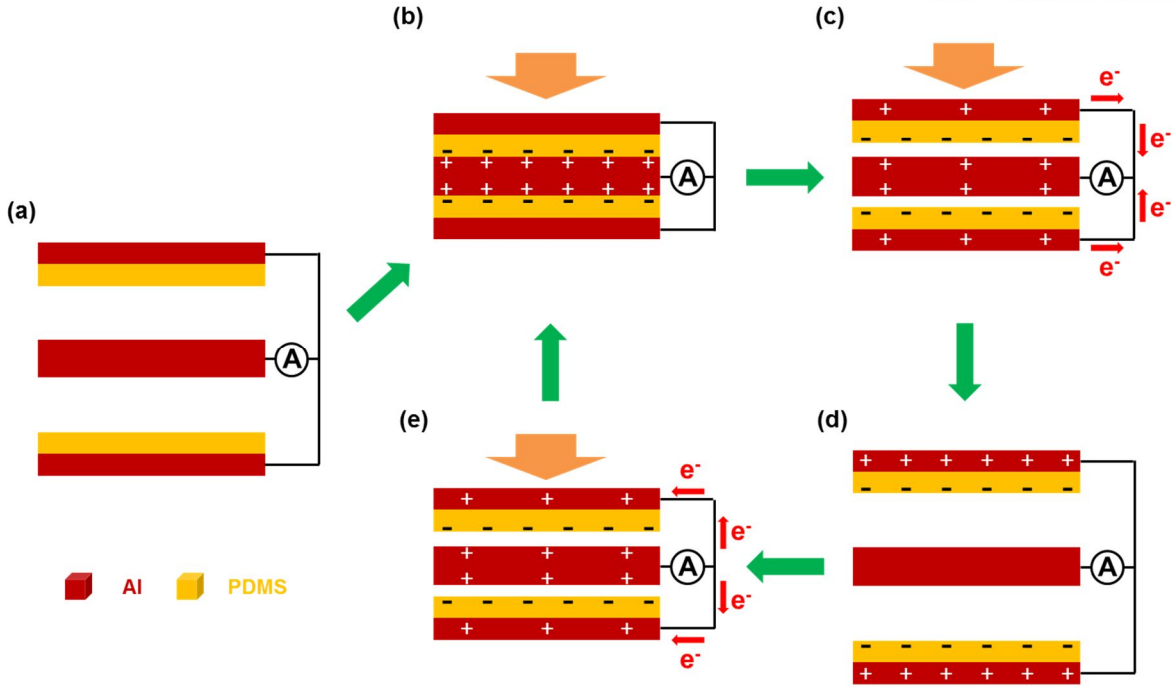

Figure 14 Mechanism of tube structured triboelectric nanogenerator. (a) Original position of tube strucutured triboelectric nanogenerator. (b) Applied vertical strain results in the contact between PDMS tube and Al wire, generating negative charges on the Al wire and positive charges on the PDMS tube. (c) Separated condition because of withdrawal of the strain. Free electrons flow from back electrode to Al wire. (d) Fully separation of the tube structured triboelectric nanogenerator. (e) Reapplied vertical strain results in the reverse flow of the free electrons.

ULSAN NATIONAL INSTITUTE OF
SCIENCE AND TECHNOLOGY

3.2.2 Cable and Textile structured triboelectric nanogenerator

A tube structured triboelectric nanogenerator was also made as a form of cable structured triboelectric nanogenerator, and the output power was measured in a same fashion. In Figure 15a, the cable structured triboelectric generator was fabricated by fixing the several tube structured triboelectric generator having a diameter of 5 mm using the PDMS in parallel connection. By connecting the three tube structured triboelectric generators in parallel, the output voltage is almost same (Figure 15b). However, in case of output current, the superposition and enhancement is observed due to electrically parallel connection among the tube structured triboelectric generators as indicated in Figure 15c.

ULSAN NATIONAL INSTITUTE OF SCIENCE AND TECHNOLOGY

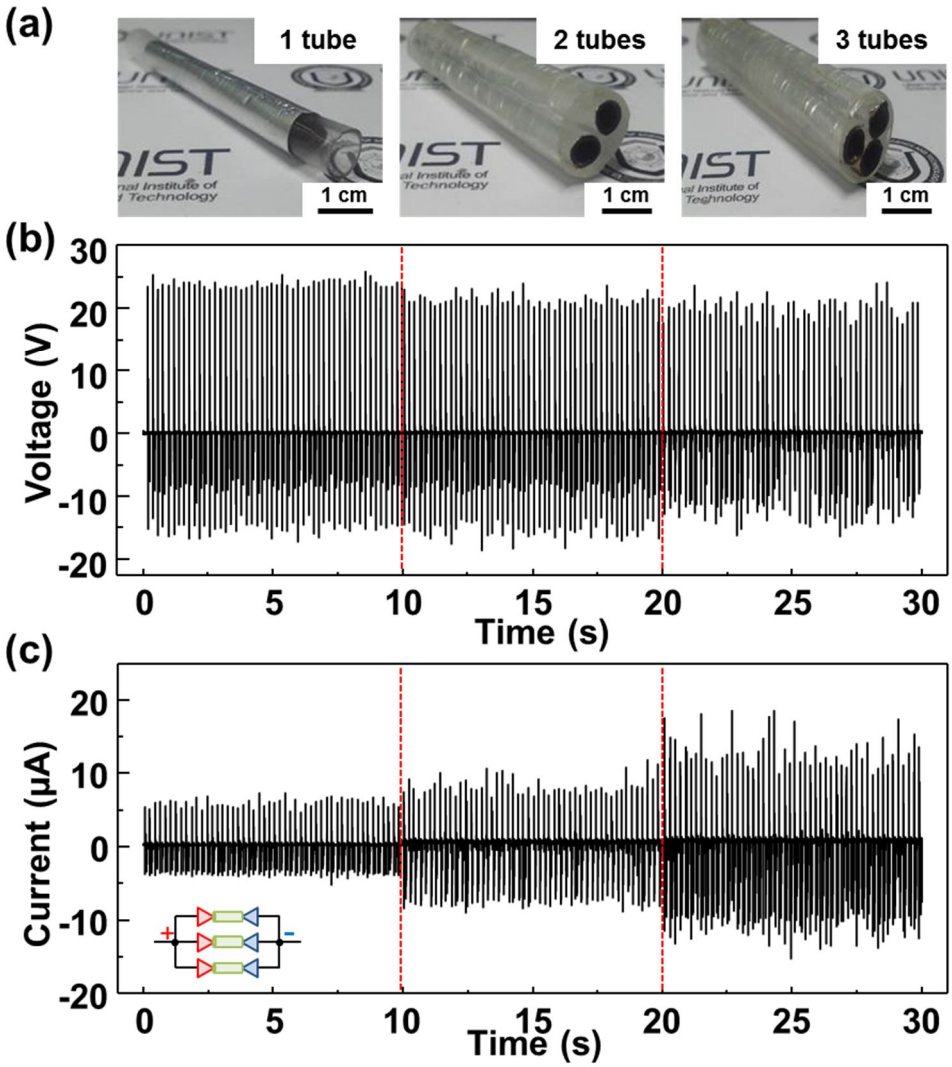

Figure 15 Cable structured triboelectgric nanogenerator. (a) Photographs of the cable structured triboelectric nanogenerator consisting of 1~3 tube structured triboelectric nanogenerator in parallel connection. (b) output voltage, (c) output current of cable structured triboelectric nanogenerator.

ULSAN NATIONAL INSTITUTE OF
SCIENCE AND TECHNOLOGY

In addition, the 15 x 15 and 30 x 30 textile structured triboelectric generators were also fabricated by weaving the thirty and sixty tube structured triboelectric generators in parallel connection respectively (Figure 16a). Figures 16b and 16c show the schematic image and photograph of the 15 x 15 textile structured triboelectric generator. The generated output voltage will remain on the almost same level (Figure 16d). However, the excessive enhancement in output current is observed. The maximized voltage and current of the textile structured triboelectric generator are 50 V and 220 μA respectively. The upper results may show the great possibility of application in wearable electronics (Figure 16e).

ULSAN NATIONAL INSTITUTE OF SCIENCE AND TECHNOLOGY

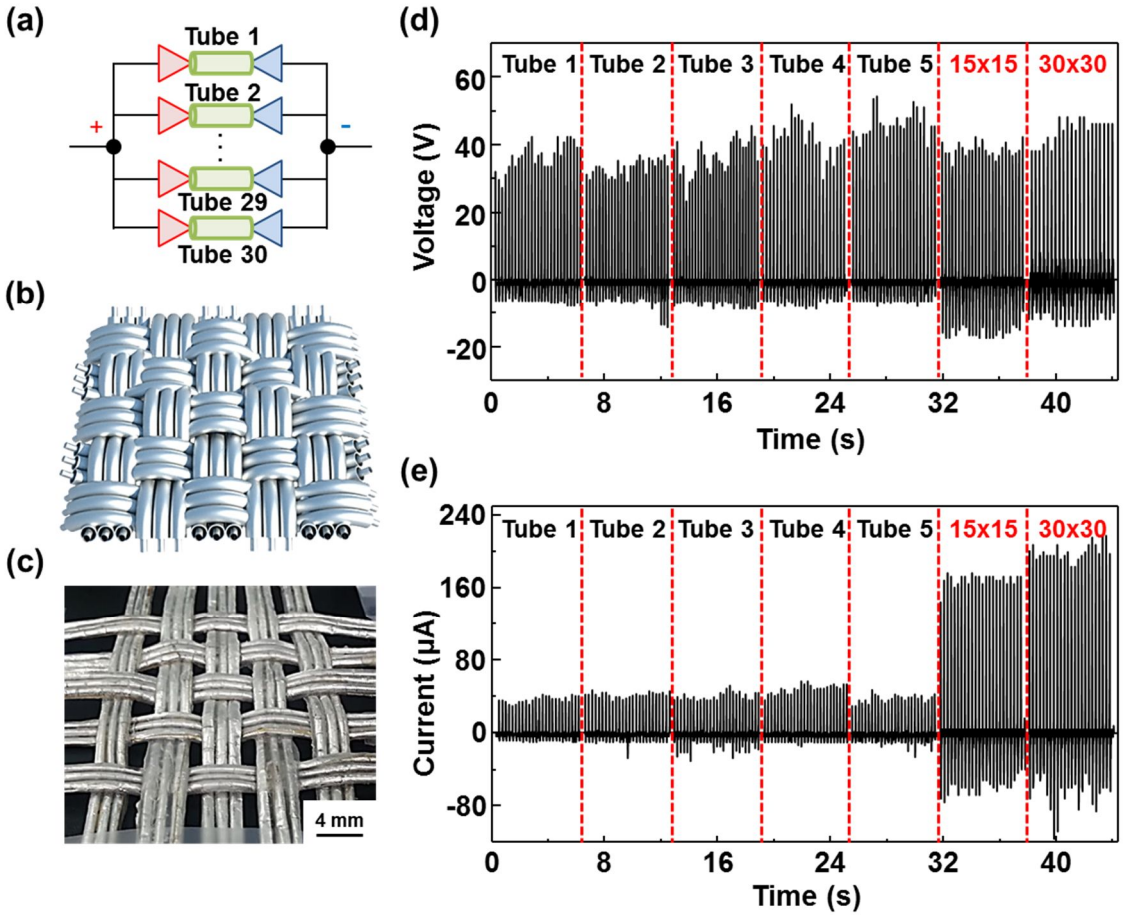

Figure 16 (a) Schematic circuit and (b) image of textile structured triboelectric nanogenerator in parallel connection. (c) Photograph of textile structured triboelectric nanogenerator. (d) Ouput voltage and (e) output current of textile structured triboelectric nanogenerator.

ULSAN NATIONAL INSTITUTE OF
SCIENCE AND TECHNOLOGY

3.2.3 Stretchability of textile structured triboelectric nanogenerator

Additionally, in order to verify the stretchability of the 15 x 15 textile structured triboelectric nanogenerator, it was stretched up to the strain of about 20% along the both sides in Figure 17. Figure 17a indicates an optical photograph of the textile structured triboelectric generator under the strain of 20 % along the diagonal direction. Figure 17b shows schematic images of deformation in the tube structured triboelectric generator applied on the stretching along the both sides. Dimension of width, denoted as diameter of the tube structured triboelectric generator will contract in response to elongation along the length direction.

ULSAN NATIONAL INSTITUTE OF SCIENCE AND TECHNOLOGY

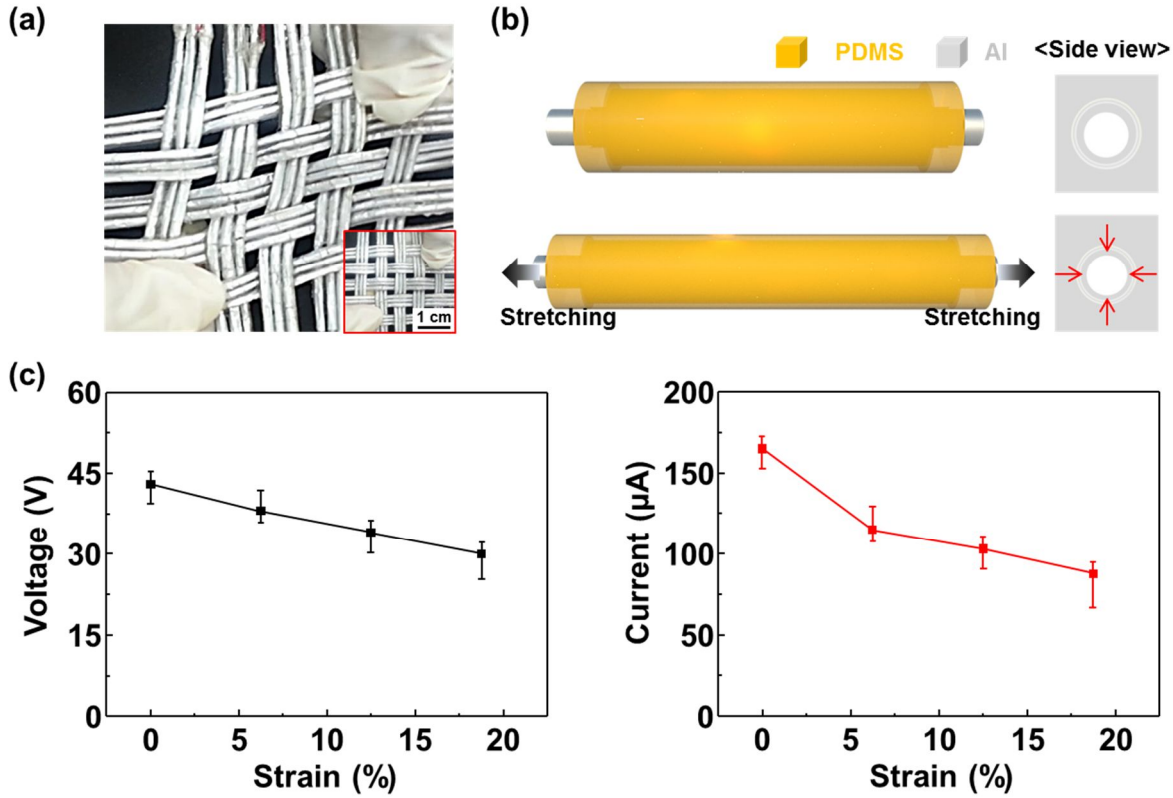

Figure 17 (a) Optical photograph of textile structured triboelectric nanogenerator under the strain 20 % along the both sides direction. (b) Schematic image of diameter change under the stretching. (c) Change of output voltage and output current of textile structured triboelectric nanogenerator.

ULSAN NATIONAL INSTITUTE OF
SCIENCE AND TECHNOLOGY

In Figure 18, the diameter of the tube structured triboelectric generator decrease as function of the increase of strain along the both sides. And because of the decrease of diameter inducing the stretching along the both sides, the output performance of textile structured triboelectric generator decreases along the increase of strain as shown in Figure 17c.

ULSAN NATIONAL INSTITUTE OF
SCIENCE AND TECHNOLOGY

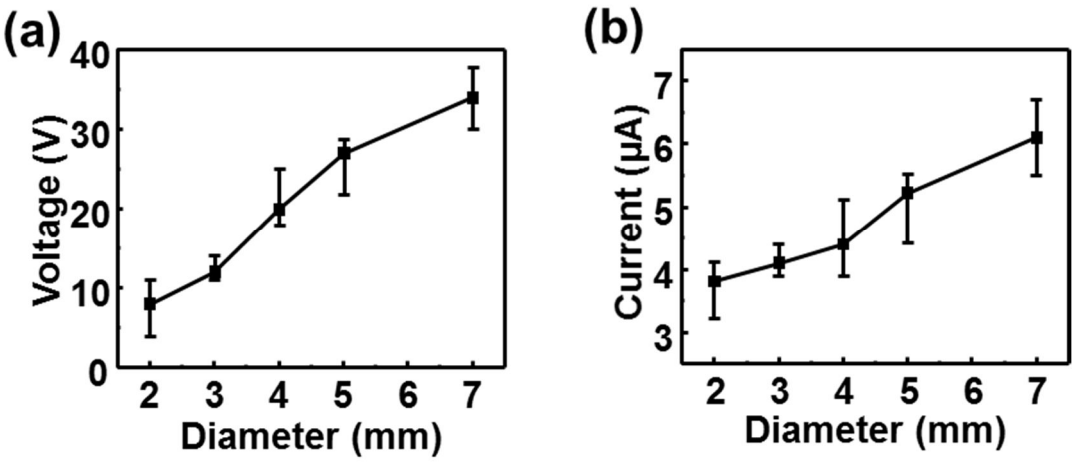

Figure 18 (a) Output voltage and (b) output current versus the diameter of tube structured triboelectric nanogenerator

ULSAN NATIONAL INSTITUTE OF
SCIENCE AND TECHNOLOGY

IV. Conclusions

In summary, we demonstrated silk fibroin-based biodegradable composite-type nanogenerators with controllable lifetime for powering to the implantable devices. And We also studied new textile-structured triboelectric nanogenerators for powering to the wearable devices. The composites are fabricated as 2D thin films and 1D wires by using a silk fibroin solution and lead-free ferroelectric (BaTiO3, ZnSnO3, BNKT, and KNN:Mn) nanoparticles. The piezoelectric output voltage and current density reached 2.2 V and 0.12 μA/cm2 in the silk fibroin composite thin film, and 1.8 V and ~ 0.1 μA/cm2 in the wire under the motion of a foot step when 30 wt% KNN:Mn nanoparticles are dispersed. Here, Ag nanowires and PVP are used to enhance the dispersion of the nanoparticles and it is also thought that the PVP prevents Ag nanowires from connecting with each other, reducing the conductivity of the composite film. A series of composite nanogenerators with different nanoparticles were fabricated and showed that the composite generator with KNN:Mn generated the largest output power because of the largest piezoelectric coupling figure of merit. Additionally, the lifetime of the device can be also controlled in water with glycerol concentration up to 48 hrs. And we also fabricated textile structured triboelectric nanogenerator through weaving a number of tube structrued triboelectric nanogenerator consisting of nanostrucuted PDMS tube and Au decorated Al wire. Large output voltage and current of textile structured triboelectric nanogenerator is about 50 V and 220 μA in the 30 x 30 textile structured triboelectric nanogenerator. Thus, the above self-powered devices have great potential for powering to the implantable and wearable electronic device and the future smart clothing industry.

ULSAN NATIONAL INSTITUTE OF
SCIENCE AND TECHNOLOGY

ACKNOWLEDGEMENT

This work was financially supported by the National Research Foundation of Korea (NRF) grant funded by the Ministry of Education, Science and Technology (MEST) (2012R1A2A1A01002787, 2010-0015035), and by the Pioneer Research Center Program through the National Research Foundation of Korea funded by the Ministry of Science, ICT & Future Planning (NRF-2013M3C1A3063602).

ULSAN NATIONAL INSTITUTE OF SCIENCE AND TECHNOLOGY

REFERENCES

1. Z.L. Wang, J. Song, Science. 312 (2006) 242-246.
2. S. Xu, Y. Qin, C. Xu, Y. Wei, R. Yang, Z.L. Wang, Nat. Nanotechnol. 5 (2010) 366-373.
3. R. Yang, Y. Qin, L. Dai, Z.L. Wang, Nat. Nanotechnol. 4 (2009) 34-39.
4. G. Zhu, R. Yang, S. Wang, Z.L. Wang, Nano Lett. 10 (2010) 3151-3155.
5. Y. Hu, Y. Zhang, C. Xu, G. Zhu, Z.L. Wang, Nano Lett. 10 (2010) 5025-5031.
6. Y. Hu, Y. Zhang, C. Xu, L. Lin, R.L. Snyder, Z.L. Wang, Nano Lett. 11 (2011) 2572-2577.
7. C. Dagdeviren, S.-W. Hwang, Y. Su, S. Kim, H. Cheng, O. Gur, R. Haney, F.G. Omenetto, Y. Huang, J.A. Rogers, Small. 9 (2013) 3398-3404.
8. K.-I Park, M. Lee, Y. Liu, S. Moon, G.-T. Hwang, G. Zhu, J.E. Kim, S.O. Kim, D.K. Kim, Z.L. Wang, K.J. Lee, Adv. Mater. 24 (2012) 2999-3004.
9. J.H. Jung, C.-Y. Chen, B.K. Yun, N. Lee, Y. Zhou, W. Jo, L.–J. Chou, Z.L. Wang, Nanotechnology. 23 (2012) 375401-375406.
10. C.K. Jeong, K.–I. Park, J. Ryu, G.–T. Hwang, K.J. Lee, Adv. Funct. Mater. 24 (2014) 2620-2629.
11. K.Y. Lee, D. Kim, J.–H. Lee, T.Y. Kim, M.K. Gupta, S.–W. Kim, Adv. Funct. Mater. 24 (2014) 37-43.
12. J.H. Jung, M. Lee, J.–I. Hong, Y. Ding, C.-Y. Chen, L.–J. Chou, Z.L. Wang, ACS Nano. 5 (2011) 10041-10046.
13. M. Yuan, L. Cheng, Q. Xu, W. Wu, S. Bai, L. Gu, Z. Wang, J. Lu, H. Li, Y. Qin, T. Jing, and Z.L. Wang, Adv. Mater., (2014) online published
14. Z. Li, G. Zhu, R. Yang, A.C. Wang, Z.L. Wang, Adv. Mater. 22 (2010) 2534–2537.
15. G.–T. Hwang, H. Park, J.–H. Lee, S. Oh, K.-I. Park, M. Byun, H. Park, G. Ahn, C.K. Jeong, K. No, H. Kwon, S.-G. Lee, B. Joung, K.J. Lee, Adv. Mater. 26 (2014) 4880–4887.
16. Q. Zheng, B. Shi, F. Fan, X. Wang, L. Yan, W. Yuan, S. Wang, H. Liu, Z. Li, Z.L. Wang, Adv. Mater. 26 (2014) 5851-5856.
17. O. Ohnishi, H. Kishie, A. Iwamoto, Y. Sasaki, T. Zaitsu, T. Inoue, Ultrasonics symposium. 1 (1992) 483-488.

ULSAN NATIONAL INSTITUTE OF SCIENCE AND TECHNOLOGY

18. B.D. Lawrence, M. Cronin-Golomb, I. Georgakoudi, D.L. Kaplan, F.G. Omenetto Biomacromolecules. 9 (2008) 1214-1220.
19. S.T. Parker. P. Domachuk, J. Amsden, J. Bressner, J.A. Lewis, D.L. Kaplan, F.G. Omenetto, Adv. Mater. 21 (2009) 2411-2415.
20. H. Perry, A. Gopinath, D.L. Kaplan, L.D. Negro, F.G. Omenetto, Adv. Mater. 20 (2008) 3070-3072.
21. C.W. Ahn, S.S. Won, A. Ullah, S.Y. Lee, S.D. Lee, J.H. Lee, W. Jo, I.W. Kim, Curr. Appl. Phys. 12 (2012) 903-907.
22. S.Y. Lee, C.W. Ahn, A. Ullah, H.J. Seog, J.S. Kim, S.H. Bae, I.W. Kim, Curr. Appl. Phys. 11 (2011) S266-S269.
23. D.-S. Leem, A. Edwards, M. Faist, J. Nelson, D.D.C. Bradley, J.C.d. Mello, Adv. Mater. 23 (2011) 4371-4375.
24. L. Hu, H.S. Kim, J.-Y. Lee, P. Peumans, Y. Cui, ACS Nano. 4 (2010) 2955-2963.
25. C.-H. Liu, X. Yu, Nanoscale. Res. Lett. 6 (2011) 75-82.
26. W. Zheng, X. Lu, W. Wang, Z. Wang, M. Song, Y. Wang, C. Wang, Phys. Stat. Sol. (a). 207 (2010) 1870–1873.
27. T. Liu, A.L. Ding, X.Y. He, X.S. Zheng, Phys. Stat. Sol. (a). 203 (2006) 3861–3867.
28. D.M. Lin, K.W. Kwok, H.Y. Tian, H. Chan, J. Am. Ceram. Soc. 90 (2007) 1458–1462.
29. Y.G. Lv, C.L. Wang, J.L. Zhang, M.L. Zhao, M.K. Li, H.C. Wang, Materials Letters. 62 (2008) 3425–3427.
30. Y. Qi, C. McAlpine, Energy Environ. Sci. 3 (2010) 1275-1285.
31. R. A. Islam, S. Priya, Appl. Phys. Lett. 88 (2006) 032903-032905.
32. M. Bichurin, V. Petrov, A. Zakharov, D. Kovalenko, S.C. Yang, D. Maurya, V. Bedekar, S. Priya, Materials. 4 (2011) 651-702.
33. S. Lu, X. Wang, Q. Lu, X. Zhang, J.A. Kluge, N. Uppal, F.G. Omenetto, D.L. Kaplan, Biomacromolecules. 11 (2010) 143-150.

ULSAN NATIONAL INSTITUTE OF
SCIENCE AND TECHNOLOGY